

# Supplementary Material for “Near-light Photometric Stereo with Symmetric Lights”

Lilika Makabe, *Student Member, IEEE*, Heng Guo, Hiroaki Santo, *Member, IEEE*,  
Fumio Okura, *Member, IEEE*, and Yasuyuki Matsushita, *Senior Member, IEEE*



To further assess the proposed method, in this supplementary material,

- 1) we add a detailed description on number of linear independencies of constraints,
- 2) we provide an additional experimental study on light fall-off relaxation,
- 3) we evaluate our method for non-Lambertian reflectance,
- 4) we discuss the estimation accuracy with varying light-to-camera offsets along  $z$ -axis,
- 5) we show albedo estimation results on the real-world dataset, and
- 6) we provide further analysis on uniform light radiance in our real-world experiment.

## 1 LINEAR INDEPENDENCIES OF CONSTRAINTS

$$\left\{ \begin{array}{l} \text{rank}(\mathbf{A}) = 2n_{\text{pairs}} - 3 \\ \text{rank}(\mathbf{A}'_{1A}) = n_{\text{pairs}} - 2 \quad (\text{non-ring light}) \\ \text{rank}(\mathbf{A}'_{1B}) = n_{\text{pairs}} - 1 \quad (\text{ring light}) \\ \text{rank}(\mathbf{A}'_{2A}) = n_{\text{pairs}} - 2 \quad (xyz\text{-axis offset}) \\ \text{rank}(\mathbf{A}'_{2B}) = n_{\text{pairs}} - 1 \quad (z\text{-axis offset}) \end{array} \right. .$$

Elementary operations of adding one row with scaling to another row do not alter the original matrix rank. First,  $2n_{\text{pairs}}$  independent equations are given by Eq. (2). Eq. (4) and Eq. (7) are obtained by taking the difference and summation of these  $2n_{\text{pairs}}$  equations, respectively, giving  $n_{\text{pairs}}$  independent equations each. Eq. (6) from Eq. (4) uses two basis and Eq. (7) uses one to eliminate unknowns from equations, leading to  $n_{\text{pairs}} - 2$  and  $n_{\text{pairs}} - 1$  independent equations, respectively, leading to  $\text{rank}(\mathbf{A})$  to be  $2n_{\text{pairs}} - 3$ .

Similarly, Eq. (13) and (14) are also obtained by Eq. (11), and use two or one basis, respectively, to eliminate unknowns in the original equation, leading to  $\text{rank}(\mathbf{A}'_{1A}) = n_{\text{pairs}} - 2$  and  $\text{rank}(\mathbf{A}'_{1B}) = n_{\text{pairs}} - 1$  in total. Similar analysis can be applied to  $\text{rank}(\mathbf{A}'_{2A})$  and  $\text{rank}(\mathbf{A}'_{2B})$ .

In the special case where all lights are on the same line, Eq. (6) from Eq. (4) needs only one basis to eliminate unknowns from equations since all the lights span in a line, leading to  $\text{rank}(\mathbf{A})$  to be  $2n_{\text{pairs}} - 2$ . With the constraint of  $\mathbf{A}'_{2B}$ , whose rank is

$n_{\text{pairs}} - 1$ . In total,  $3n_{\text{pairs}} - 3$  constraints can be introduced, and thus light-to-surface distances can be recovered with at least  $2n_{\text{pairs}}$ , which is the minimum setting for a *line* light.

## 2 LIGHT FALL-OFF RELAXATION ANALYSIS

In Sec. 4.2 in the main paper, we evaluate the effect of the light fall-off relaxation using  $n_{\text{pairs}} = 4$  light arrangement from Fig.12 used in the synthetic experiments. While the experiment in the main paper only shows results of normal estimation accuracy by varying light-to-surface distances, we here analyze the applicability of this relaxation. By rewriting Eq. (8) in the main paper using  $d_* = \|\mathbf{s}_* - \mathbf{x}\|_2$ , where  $\mathbf{s}_*$  and  $\mathbf{x}$  respectively denote the point light source and surface positions, our light fall-off relaxation including the normalization factor is read as:

$$\frac{1}{d_*^3} \approx \frac{1}{d_*^2}. \quad (1)$$

Since we solve the homogeneous system to obtain light-to-surface distances  $e_* = \rho^{-1}d_*^2$ , the solutions naturally involve ambiguity. When the nullity of the design matrix is 1, the solutions are obtained up to scale. Namely, the light fall-off approximation yields a solution equivalent to the one without the approximation if  $\mathbf{d}^2 = k\mathbf{d}^3$  holds, where  $\mathbf{d}_*^p = [d_1^p, \dots, d_N^p]^T$ ,  $k \in \mathbb{R}$ , and  $N = 2n_{\text{pairs}}$  is the number of light sources. Given the two light indices  $i, j$ , the following metric approaches 1 if the relaxation well approximates the unrelaxed light fall-off term:

$$\frac{\frac{d_j^3}{d_i^3}}{\frac{d_j^2}{d_i^2}} = \frac{d_j}{d_i} \approx 1. \quad (2)$$

To assess the error by the relaxation, we evaluate the error  $r$  of light fall-off terms between  $1/d^2$  and  $1/d^3$  case defined as

$$r \triangleq \text{mean}_i \left( \left( \frac{d_i}{d_1} \right) - 1 \right)^2, \quad (3)$$

where  $i = 2, \dots, 2n_{\text{pairs}}$ .

Figure S1 visualizes the relative error  $r$  at varying point locations  $\mathbf{x}$  with respect to the camera and field of views (FOVs) associated with their focal lengths. For the visualization purpose, we only consider a slice of the view volume on the  $x$ - $z$  plane. Other experimental settings are the same as the synthetic experiments in the main paper, *e.g.*, resolution.

If we allow 2% error, *i.e.*,  $r = 0.02$ , in the case of focal length  $f = 85$  mm, for example, we should keep the depth  $z \geq 3.54$ ,

• L. Makabe, H. Guo, H. Santo, F. Okura, and Y. Matsushita are with Graduate School of Information Science and Technology, Osaka University, Japan.  
E-mail: {lilika.makabe, heng.guo, santo.hiroaki, okura, yasumat}@ist.osaka-u.ac.jp

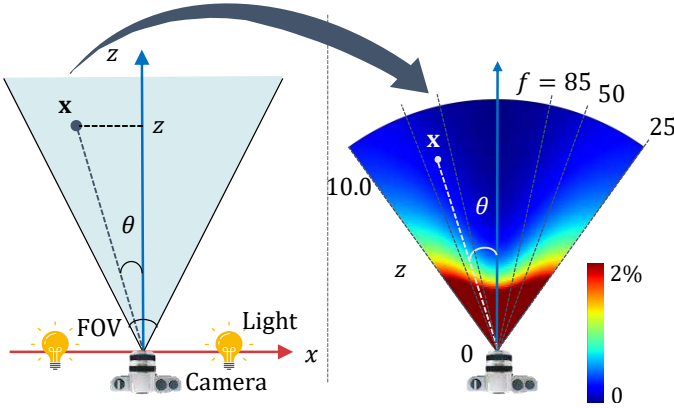


Fig. S1: The left-hand side illustrates the lights and 3D point  $\mathbf{x}$  in the camera coordinate system looked from the bird-view. The blue area shows the field of view (FOV) of the camera, and  $\theta$  is an angle between the optical axis and a camera ray going through the 3D point  $\mathbf{x}$ . The right-hand side shows the heatmap of the light fall-off approximation error  $r$ . The dotted lines indicate FOV for focal lengths of  $f = 25, 50, 85$  mm.

which supports the result in Sec. 4.2 in the main paper. For a shorter focal length, we need to put the target object further away to ensure that the relative error  $r \leq 0.025$  at all the points within the FOV, e.g.,  $z \geq 2.73$  for  $f = 50$  and  $z \geq 2.53$  for  $f = 25$ .

### 3 RESULTS ON NON-LAMBERTIAN SURFACE

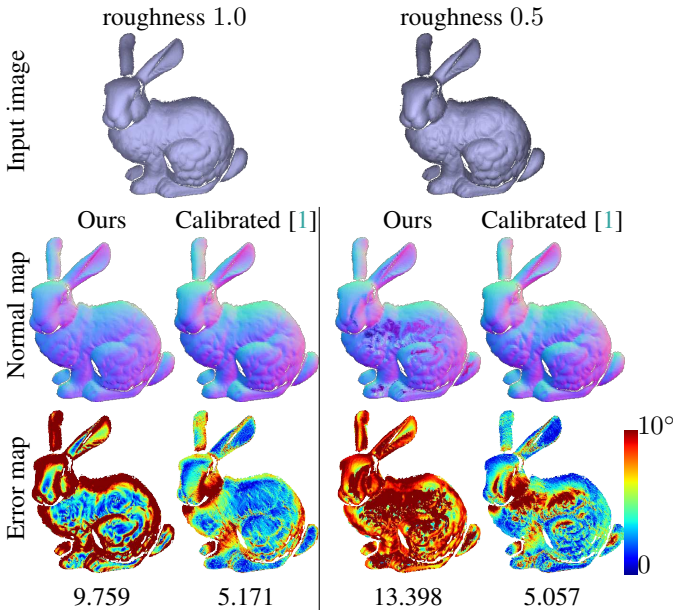


Fig. S2: Estimation results with varying roughness values. We show the estimated surface normal together with angular error maps, under varying roughness values in Disney Principled BSDF model. [2]

To examine the effect of a different reflectance model, we evaluate our method with a scene rendered using Disney’s Principled BSDF model [2]. We ignore the clearcoat term and set the specular value to 0.5 and roughness values to 0.5 and 1.0. Figure S2 shows the results of the estimated normal maps from ours and

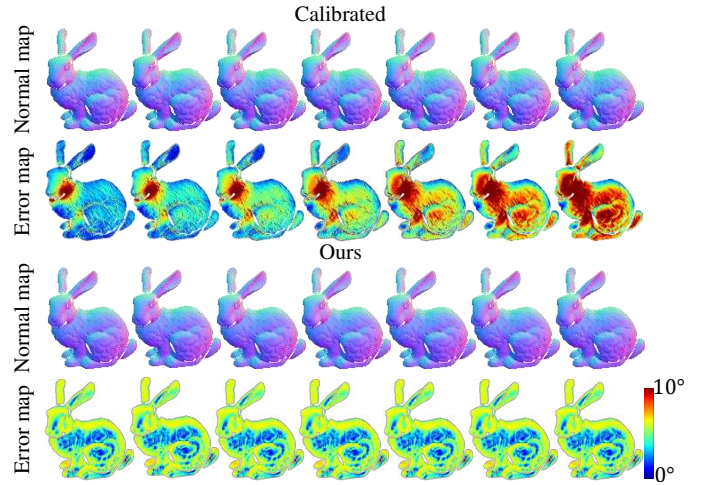
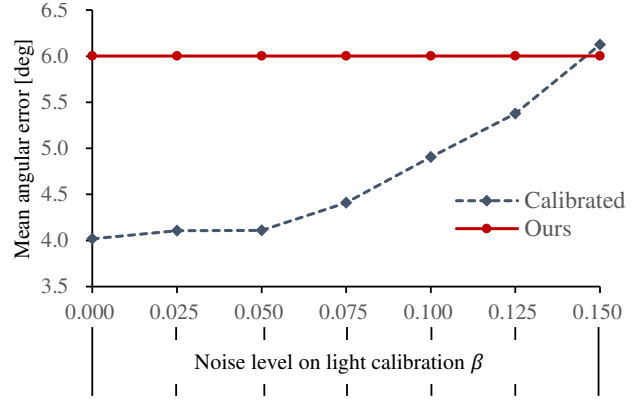


Fig. S3: Estimation results on our synthetic dataset with adding an error  $\beta$  to the light-to-camera positions. The plot shows mean angular errors by the proposed method (Ours) and the comparison method (Calibrated) with varying error  $\beta$ . Below the plot, we show the corresponding estimation of the surface normal, along with the angular error map by both methods. The calibrated method is significantly affected by the inaccurate calibration, while the proposed method is not affected by the light calibration results.

Calibrated. Although in the roughness = 0.5 case, our method fails to estimate the correct normal map due to the deviation from the Lambertian assumption, we still obtain reasonable estimation in the roughness = 1.0 case, even though the modeling of the diffuse reflectance is different from that of Lambertian.

### 4 RESULTS ON VARYING LIGHT-TO-CAMERA OFFSET

In a geometric light source calibration, the light position along the  $z$ -axis in the camera coordinates, i.e., light-to-camera offset  $s_z$ , is known to be sensitive to noise due to the narrow-baseline triangulation [3], [4].

In this section, we evaluate how the light’s geometric calibration error impacts the surface normal estimation by the calibrated photometric stereo method [1], while it does not affect our method at all.

We render synthetic images, where the light-to-surface and light-to-camera distances are set to 6 and 0, respectively, and use  $n_{\text{pairs}} = 4$  lights as shown in Fig. 5. Figure S3 shows the estimated results of the calibrated method with Gaussian noise added with varying standard deviations  $\beta$  to the light source

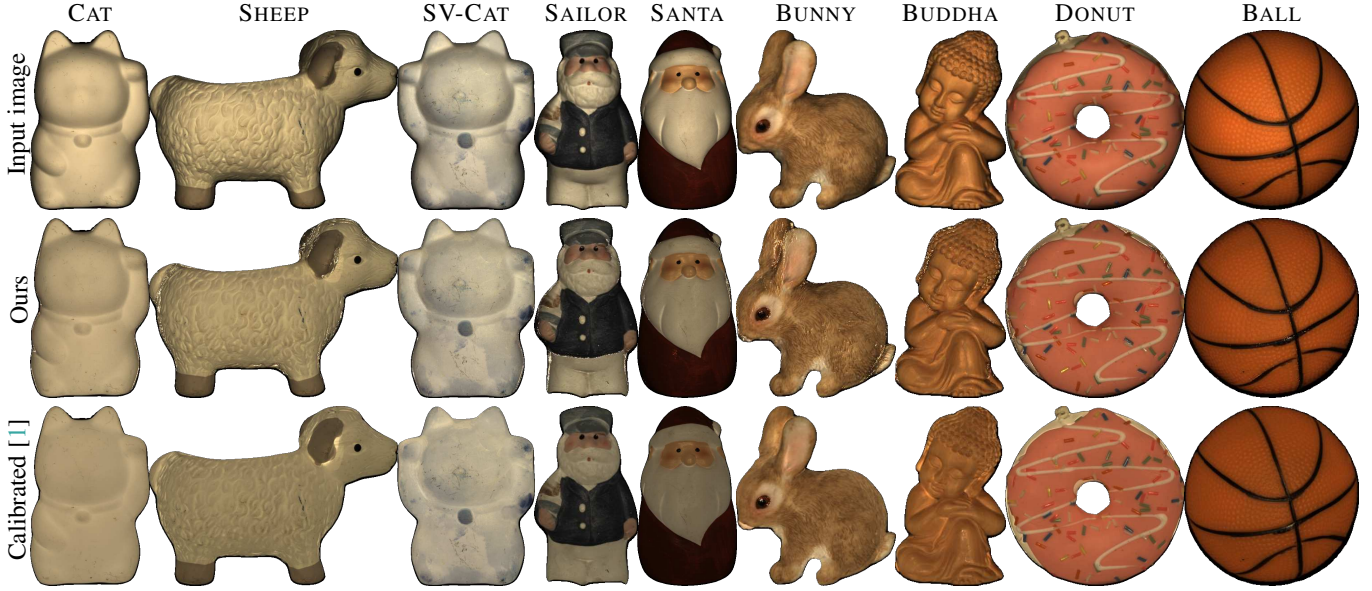


Fig. S4: Estimated albedo maps for our real-world dataset. For each scene, we show one of the input images and estimate albedo maps by the proposed method (Ours) and Calibrated.

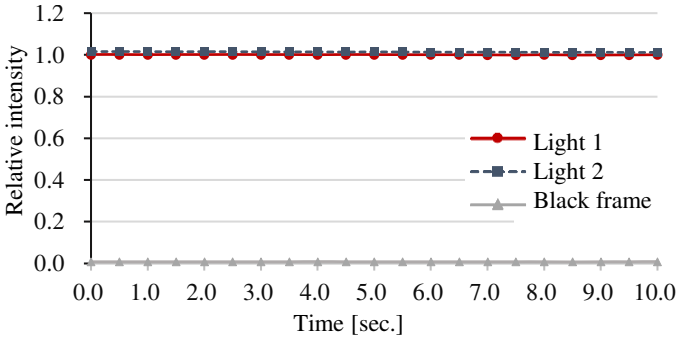


Fig. S5: The intensities of two different LED devices, LED1 and LED2, and ambient illumination. Each data point represents the mean intensity of a  $100 \times 100$  pixel patch taken from the center of the captured image.

positions. While the calibrated method estimates accurate surface normals with accurate light calibration, if calibration becomes inaccurate, the shape errors increase rapidly. The varying light-to-camera offset does not affect our estimation results, highlighting one of the advantages of the proposed method that does not rely on light source calibration.

## 5 ALBEDO ESTIMATION RESULTS ON THE REAL-WORLD DATASET

Figure S4 shows the estimated albedo maps corresponding to the surface normal estimations shown in Sec. 5 in the main paper. For visualization, we scale the albedo values using the mean image of all eight input images, so that the median of the estimated albedo map should be equal to that of the mean image. Although both the calibrated and proposed methods suffer from some specular reflection, overall, our albedo estimations are comparable to the calibrated method.

## 6 LIGHT RADIANCE ANALYSIS

Light radiance is assumed to be uniform for all light sources as we employ a constant current circuit in our device. To further verify that, we use a CCD camera and Lambertian calibration board, and measure the light intensities of two LED devices fixed in the same position, by swapping the device. Figure S5 presents the measured intensities of LED1, LED2, and ambient illumination, providing a visual representation of their stability over time. The mean intensities over 10 seconds are 1.00 and 1.01, respectively, where the intensities are scaled so that the mean intensity of LED1 should be 1. Also, the corresponding standard deviations are  $8.33 \times 10^{-4}$  and  $1.56 \times 10^{-3}$ . These statistics indicate that the oscillation in intensity over time and between devices is negligible.

## APPENDIX

**Proposition 1.** *the point  $\mathbf{x} \in \mathbb{R}^n$  which has the known ratio  $d_1, d_2 \in \mathbb{R}$  ( $d_1 > d_2$ ) of distances to the fixed points  $\mathbf{p}_1, \mathbf{p}_2 \in \mathbb{R}^n$  lies in the sphere whose center and radius are  $\frac{d_1^2 \mathbf{p}_2 - d_2^2 \mathbf{p}_1}{d_1^2 - d_2^2}$  and  $\frac{d_1 d_2}{d_1^2 - d_2^2} \|\mathbf{p}_1 - \mathbf{p}_2\|_2^{\frac{1}{2}}$ , respectively.*

*Proof of Proposition 1.* We can rewrite the condition on the distances between  $\mathbf{x}$  and fixed points as:

$$\|\mathbf{x} - \mathbf{p}_1\|_2^1 : \|\mathbf{x} - \mathbf{p}_2\|_2^1 = d_1 : d_2. \quad (4)$$

From the above equation, we transform into one sphere equation as:

$$d_1^2 (\mathbf{x} - \mathbf{p}_2)^\top (\mathbf{x} - \mathbf{p}_2) = d_2^2 (\mathbf{x} - \mathbf{p}_1)^\top (\mathbf{x} - \mathbf{p}_1)$$

$$i.f.f. \left\| \mathbf{x} - \frac{d_1^2 \mathbf{p}_2 - d_2^2 \mathbf{p}_1}{d_1^2 - d_2^2} \right\|_2^2 = \frac{d_1^2 d_2^2}{(d_1^2 - d_2^2)^2} \|\mathbf{p}_1 - \mathbf{p}_2\|_2^2,$$

whose center and radius are  $\frac{d_1^2 \mathbf{p}_2 - d_2^2 \mathbf{p}_1}{d_1^2 - d_2^2}$  and  $\frac{d_1 d_2}{d_1^2 - d_2^2} \|\mathbf{p}_1 - \mathbf{p}_2\|_2^{\frac{1}{2}}$ .  $\square$

**Proposition 2.** *When the radius of the symmetric lights  $r_*$  of every pair are the same, all the possible Apollonius spheres are centered on a line, whose direction is  $[-y', x', 0]$ .*

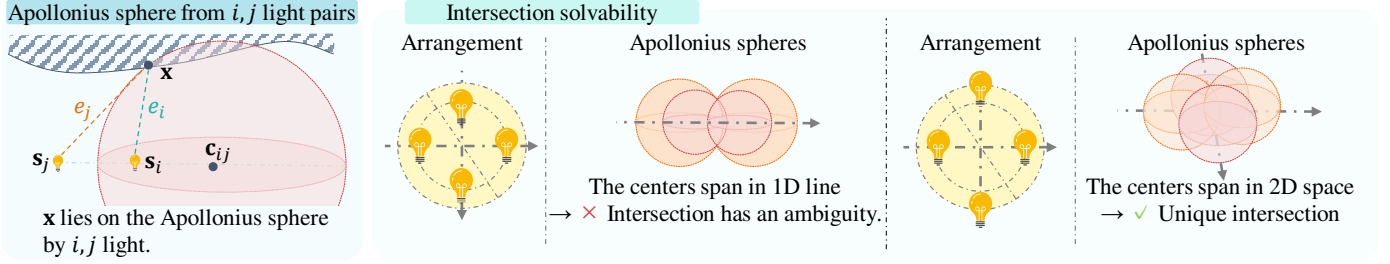


Fig. S6: Given the position and estimated light-to-surface distances of arbitrary two lights, the corresponding sphere can be drawn where the surface point  $\mathbf{x}$  lies.  $\mathbf{x}$  can be recovered as the intersection of at least 3 spheres. When every light shares the same radii, the centers of corresponding Apollonius spheres span in a 1D line, leading to an ambiguity in the intersection.

*Proof of Proposition 2.* Let us define a light position and scaled distance using a light index *e.g.*,  $\mathbf{s}_i = \mathbf{s}_{r_i}^{\theta_i}$ ,  $e_i = e_{r_i}^{\theta_i}$ , and the center of the Apollonius sphere by light indices *i, j* as  $\mathbf{c}_{ij}$  for a simplicity. We show that the directional vector between two of the Apollonius spheres is always the same, regardless of the choice of the light indices.

Given  $i^{th}$  and  $j^{th}$  light, center of the Apollonius sphere  $\mathbf{c}_{ij}$  can be represented as:

$$\begin{aligned} \mathbf{c}_{ij} &= \frac{e_i (\mathbf{s}_j - \mathbf{s}_o) - e_j (\mathbf{s}_i - \mathbf{s}_o)}{e_i - e_j} \\ &= \frac{(\mathbf{x}'^T \mathbf{x}' + 2\mathbf{x}'^T \mathbf{s}_o) (\mathbf{s}_j - \mathbf{s}_i) + r_i^2 \mathbf{s}_j - r_j^2 \mathbf{s}_i}{(r_i^2 - r_j^2) - 2\mathbf{x}'^T (\mathbf{s}_j - \mathbf{s}_i)}, \end{aligned}$$

by substituting the definition of the scaled distances in Eq (10) in the main paper. Especially when  $r_i = r_j = r$ , the center  $\mathbf{c}_{ij}$  can be further simplified as :

$$\mathbf{c}_{ij} = \frac{\mathbf{x}'^T \mathbf{x}' + 2\mathbf{x}'^T \mathbf{s}_o + r^2}{-2\mathbf{x}'^T (\mathbf{s}_j - \mathbf{s}_i)} (\mathbf{s}_j - \mathbf{s}_i).$$

When all the lights' radii  $r_i, r_j, r_k, r_l$  are the same as each other, the directional vector between two of the Apollonius spheres center  $\mathbf{c}_{ij}, \mathbf{c}_{kl}$  can be obtained as follows:

$$\mathbf{c}_{ij} - \mathbf{c}_{kl} \propto \left( \frac{(\mathbf{s}_j - \mathbf{s}_i)}{\mathbf{x}'^T (\mathbf{s}_j - \mathbf{s}_i)} - \frac{(\mathbf{s}_l - \mathbf{s}_k)}{\mathbf{x}'^T (\mathbf{s}_l - \mathbf{s}_k)} \right) \quad (5)$$

$$\propto [-y', x', 0]^T, \quad (6)$$

which is independent of the selection of light. Figure S6 illustrates the valid and invalid light arrangements with corresponding Apollonius spheres.  $\square$

## REFERENCES

- [1] Y. Quéau, B. Durix, T. Wu, D. Cremers, F. Lauze, and J.-D. Durou, "Led-based photometric stereo: Modeling, calibration and numerical solution," *Journal of Mathematical Imaging and Vision*, vol. 60, 2018.
- [2] B. Burley and W. D. A. Studios, "Physically Based Shading at Disney," in *Proceedings of SIGGRAPH*, 2012.
- [3] J. Ackermann, S. Fuhrmann, and M. Goesele, "Geometric point light source calibration," in *Proceedings of Vision, Modeling, and Visualization*, 2013.
- [4] H. Santo, M. Waechter, W. Lin, Y. Sugano, and Y. Matsushita, "Light structure from pin motion: Geometric point light source calibration," *International Journal of Computer Vision (IJCV)*, vol. 128, no. 7, pp. 1889–1912, 2020.